Chapter 4

Epitaxial Cu_3Ge Thin Film: Fabrication, Structure, and Property

Fan Wu and Nan Yao

Additional information is available at the end of the chapter

http://dx.doi.org/10.5772/64060

Abstract

In this paper, the fabrication and electrical property characterization of epitaxial Cu_3Ge thin film are performed. By adjusting deposition parameters, the crystallinity of the as-grown Cu_3Ge thin films is improved, with the formation of twins within it. The average work function of epitaxial Cu_3Ge thin film is measured to be ~4.47 + 0.02 eV, rendering it a desirable mid-gap gate metal for applications in complementary metal-oxide semiconductor (CMOS) devices. The present study therefore shows an epitaxial Cu_3Ge thin film that is promising for applications.

Keywords: Cu_3Ge thin film, sapphire, twin, pulsed laser deposition, semiconductor metallization

1. Introduction

Cu_3Ge is a promising candidate and an alternative to Cu for contacts and interconnections in advanced integrated circuit devices. It has a relatively low bulk resistivity throughout the compositional window of 25–35 at% Ge [1, 2]. Its thermal stability against oxidation is also excellent [3, 4]. Furthermore, the service life of Cu_3Ge is considerably longer than Cu because the out-diffusion of Cu [4] is reduced. Not only different substrates have been used for growth of polycrystalline Cu_3Ge films (including GaAs [5–7], Si [4, 8–10], Ge [10, 11], $YBa_2Cu_3O_{7-x}$ [12], Si_xGe_{1-x} [8, 9, 13], Ta/TaN [14] and GaN [15]), but also various deposition methods have been used for Cu_3Ge thin film fabrication. For example, multiple physical vapor deposition methods, such as electron beam deposition, sputtering [1, 2, 4, 11, 12, 16] and thermal evaporation [17], or chemical approaches such as vapor-solid reaction [14], have been exploited. Despite the achievements in this field, the Cu_3Ge films reported up to now were mostly polycrystalline with

impurity phase [1,2,4–13]. Consequently, Cu_3Ge films with better crystallinity are highly desired, in order to minimize diffusion paths (grain boundaries) and lower electrical resistivity.

In this chapter, we show the fabrication of epitaxial Cu_3Ge thin films with significantly improved crystallinity, due to a modified deposition route of Cu_3Ge thin films. The average work function of epitaxial Cu_3Ge thin film is measured to be ~4.47 + 0.02 eV, rendering it a desirable mid-gap gate metal to be used for applications in CMOS devices. Since sapphire has been widely used as a substrate in high-power and high-frequency CMOS integrated circuits, especially for high-power radio-frequency applications, the integration of Cu_3Ge as contacts or interconnections onto sapphire substrate will have potential applications in the semiconductor industry.

2. Experimental procedure

Pulsed laser deposition (PLD) was used to deposit Ge and Cu thin films repetitively on sapphire substrates. For Cu atoms to mix and bond with Ge atoms intimately, ultrathin Ge and Cu layers were deposited in each repetition. Cu_3Ge film is thus expected to have improved crystallinity as laser ablation provides excess kinetic energies of Cu/Ge atoms. A series of five Cu_3Ge films are fabricated at 400 ± 10°C, with systematically changed deposition parameters for investigating their correlation with the crystallinity of Cu_3Ge films. Specifically, 90 repetitions of Ge and Cu layers are deposited for all five samples, with a changing pulse number of Ge and Cu deposition for sample 1–5. For example, 35 pulses of Cu and five pulses of Ge are deposited in one repetition for sample 1, and a total of 90 repetitions are performed. Similarly, pulses of Cu in one repetition for sample 2–5 are 25, 15, 14, and 7, while pulses of Ge in one repetition for sample 2–5 are 5, 5, 2, and 1. Before deposition, multi-step cleaning is performed on the substrates. They are first cleaned with boiled acetone for 5 min, and then ultrasonically cleaned in acetone and methanol for 5 min each. Nitrogen gun is used to dry the cleaned substrates, which are then mounted into the chamber 4 cm away from the target. The pulsed KrF excimer laser used has a wavelength of 248 nm and pulse duration of 25 ns. The pre-deposition vacuum is $\sim 10^{-7}$ Torr, while the actual deposition vacuum is $\sim 3.0 \times 10^{-4}$ Torr due to heating. The laser source provides a laser with constant exciting voltage (23.8 keV [18–26]), and hits the pure Cu and Ge targets (from ESPI) at an incidence angle of 45°. Since the spot size of the landing laser is ~2 mm × 3 mm and the landing laser beam energy is ~0.29–0.30 J, the laser beam energy density is ~4.8–5 J cm^{-2}.

High-resolution transmission electron microscope (HRTEM) JEOL-2010F with a point-to-point resolution of 0.18 nm is used to characterize the microstructure of the deposited films. Focus ion beam (FIB) is used for preparing TEM samples. Rigaku X-ray diffractometer (XRD) is used to perform XRD θ–2θ scan analysis, with Cu-Ka X-ray source. Atomic force microscopy (AFM) is exploited to obtain height images for characterization of thin film morphology. All AFM scans are performed in tapping mode, using cantilevers with a resonance frequency close to 330 kHz. The AFM image resolution is 512 × 512 pixels, and scan rate is 1.5 × 1.5 μm^2. Gwyddion is used to process the obtained AFM images.

http://dx.doi.org/10.5772/64060

The local work function of epitaxial Cu_3Ge thin film was measured by Kelvin probe force microscopy (KPFM). In KPFM measurements, the conductive tip (NSG03/Pt) was working in tapping mode and lift mode scan. Reliable topographic images were obtained before the KPFM measurements. In KPFM tests, an AC and a DC bias were applied on the cantilever while the sample remained grounded. The frequency of the AC signal was set at ~2kHz lower than the resonance frequency of the cantilever and the amplitude AC voltage was 560 mV. The lift scan height was 50 nm and the scan rate was 0.75 Hz.

3. Results and discussion

To characterize the microstructures of the deposited thin films, XRD θ–2θ patterns are obtained and shown in **Figure 1**. Since Cu/Ge layer thickness in each repetition is decreasing from sample 1 to sample 5, the crystallinities of Cu_3Ge films are improved. The two peaks corresponding to c-sapphire (0 0 6) and (0 0 1 2) planes exist in all XRD θ–2θ patterns, showing the substrate orientation. The film of sample 1 is polycrystalline Cu_3Ge with impurity Ge phase, as evidenced by the peak at 27.32° belonging to Ge (1 1 1) plane, and multiple peaks belonging to Cu_3Ge. Note that for sample 1, the deposited Cu/Ge layers in one deposition repetition were too thick to react with each other completely, such that extra Ge phase exists. The impurity Ge phase also exists for samples 2 and 3 (as evidenced by the peak at 27.32° for Ge (1 1 1)), due to the high Ge:Cu pulse ratio in each repetition. Furthermore, the crystallinities of Cu_3Ge films are also improved for samples 2 and 3, as evidenced by the disappearance of peaks belonging to Cu_3Ge (-1 3 1) and (0 0 4) planes. For samples 4 and 5, no impurity Ge phase exists, due to the reduced pulse numbers of Ge/Cu. More importantly, the crystallinities of Cu_3Ge films are

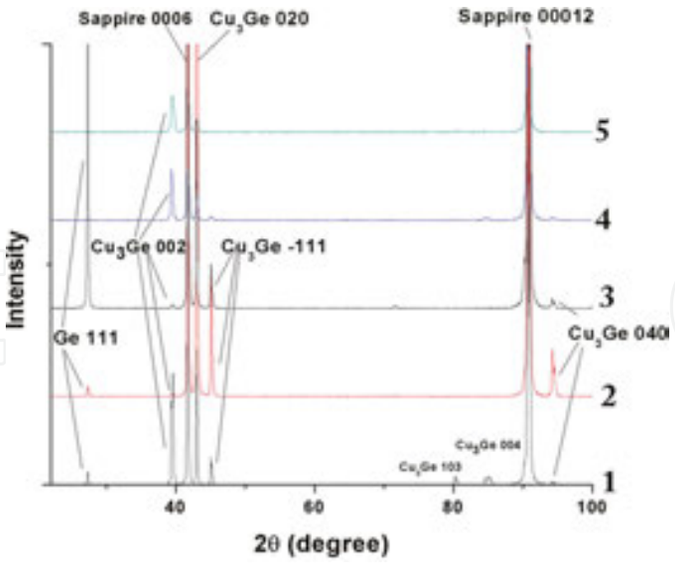

Figure 1. XRD θ–2θ patterns for samples on *c*-plane sapphire (Al_2O_3{0 0 1}). For all five samples, the laser shot frequency is 1 Hz, the deposition temperature is 400°C, and 90 repetitions of depositions of Cu/Ge were performed, while numbers of laser pulses for Cu and Ge depositions are different: sample 1: Cu:Ge=35:5; sample 2: Cu:Ge=25:5; sample 3: Cu:Ge=15:5; sample 4: Cu:Ge=14:2; and sample 5: Cu:Ge=7:1.

significantly improved with only two Cu_3Ge peaks remaining, proving that bi-epitaxial Cu_3Ge thin films have been grown on c-substrate.

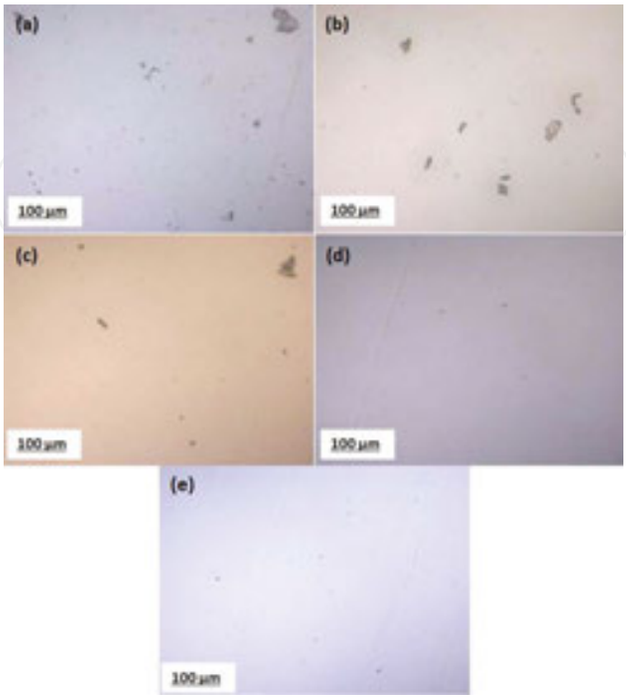

Figure 2. (a)–(e) The plan-view images of samples (1)–(5) respectively, observed by optical microscope.

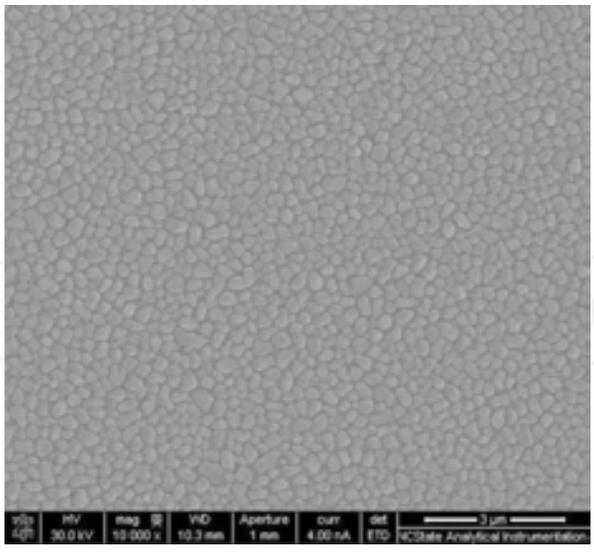

Figure 3. Typical plan-view SEM image of the Cu_3Ge film in sample 5, showing a uniform Cu_3Ge film grown via 3-D growth mode, without the formation of chunks and excessive Ge grains.

The quality and crystallinity of Cu_3Ge films in sample 1–5 are also demonstrated by the plan-view images of optical microscope images, shown in **Figure 2**. **Figure 2(a)–(e)** correspond to

the plan-view images of samples 1–5, respectively. Chunks appear in the plan-view images of samples 1, 2, and 3, possibly due to the existence of excessive Ge grains in addition to the Cu_3Ge phase. In contrast, uniform films are observed in **Figure 2(e)** and **(f)**, proving the high quality of the Cu_3Ge films with good crystallinity for samples 4 and 5. SEM and AFM analyses are performed to show more detailed surface morphology of sample 5. The plan-view SEM image (**Figure 3**) shows the surface morphology of Cu_3Ge film, with an average diameter of Cu_3Ge islands to be ~300–500 nm. The complementary AFM height map (**Figure 4**) demonstrates the average heights of Cu_3Ge islands to be ~180–240 nm.

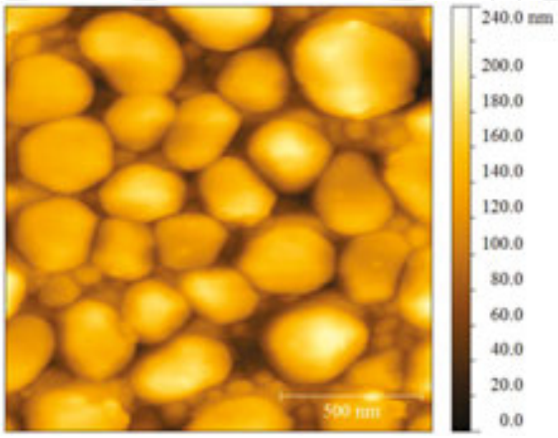

Figure 4. Typical AFM image of Cu_3Ge film on c-sapphire in sample 5, showing the diameters of these islands to be ~300–500 nm, with heights ranging from 180 to 240 nm.

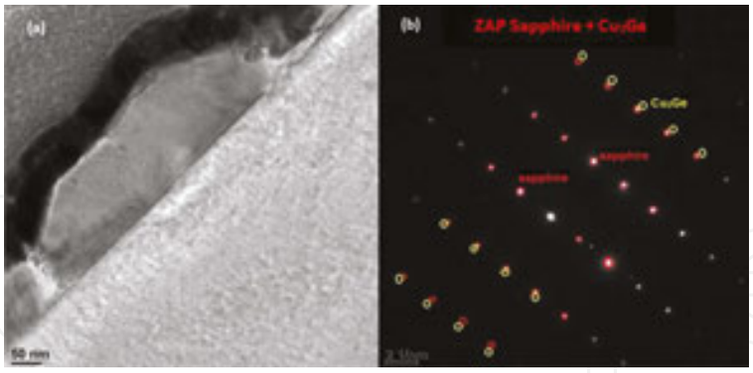

Figure 5 (a) A typical bright-field cross-section TEM image showing the film morphology of sample 5 and (b) the [1 1 0] zone-axis pattern (ZAP) of sample 5, clearly demonstrating an epitaxial relationship between the single-crystal Cu_3Ge island and c-sapphire substrate [42].

TEM is performed to further study the epitaxial film morphology, as demonstrated in **Figure 5(a)**. Note that the Au/Pt layers on top of Cu_3Ge are deposited during ample preparation for protection. Based on the morphology of the Cu_3Ge film, it may grow on the *c*-plane sapphire via 'layer-plus-island growth' mode following a two-step process. Initially, the Cu_3Ge grew in a layer-by-layer fashion on the *c*-plane sapphire to form an ultrathin uniform film up to several

monolayers thick; beyond a critical thickness, the Cu_3Ge growth continued through the nucleation and coalescence of adsorbate islands. A sharp interface without secondary phases is observed between c-sapphire and epitaxial Cu_3Ge film, over a large area. Selected area diffraction pattern (SADP) analysis (**Figure 5(b)**) was performed at the Cu_3Ge/sapphire interface for studying orientation relationships. Overlapping of the low-order diffraction points of film and substrate corroborates their epitaxial relationship. A careful examination does show the splitting of higher order diffraction points of two phases.

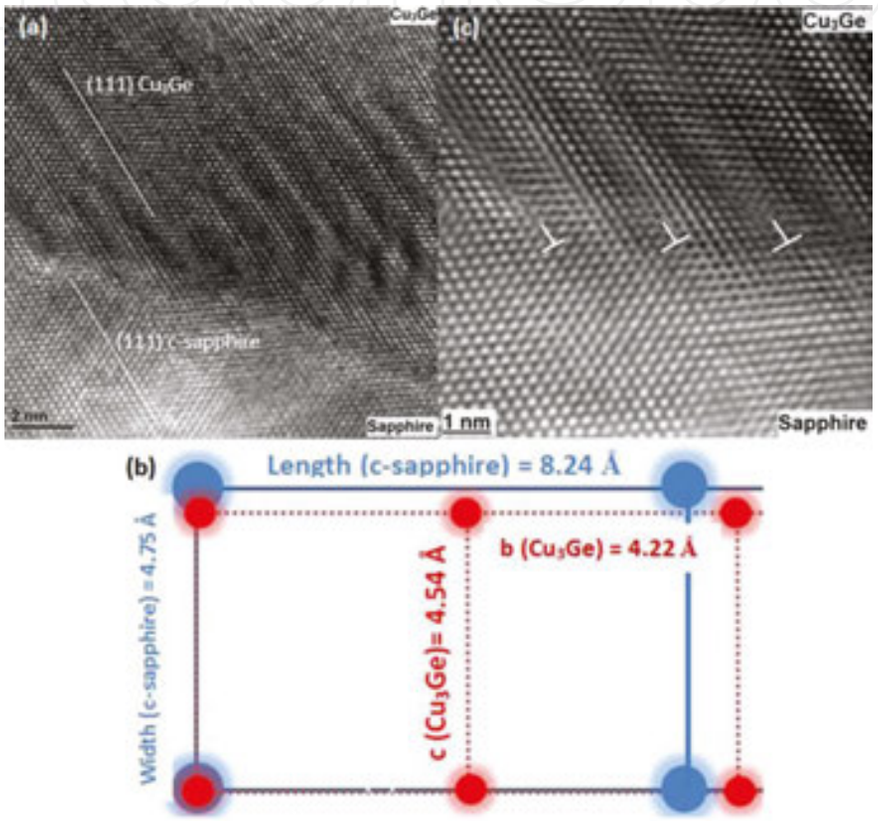

Figure 6 (a) An HRTEM image showing the atomic structure at the interface region between the Cu_3Ge island and c-sapphire substrate. The viewing direction is [1 1 0] zone of c-sapphire ([11–20] zone in Miller-Bravais Indices system), (b) the schematic illustration of the matching scenario at the interface between e_1-Cu_3Ge (0 1 0) and c-sapphire (0 0 1), and (c) the HRTEM image at a higher magnification showing the atomic structure at the interface in detail, at the region close to that of (a) [42].

HRTEM investigation was performed to study the atomic structure at the Cu_3Ge/c-sapphire interface, as shown in **Figure 6(a)**. The Cu_3Ge/c-sapphire interface is semi-coherent [27], due to visible periodic contrast along the interface induced by misfit dislocations, which accommodates the misfit strain between the two phases. For c-sapphire and Cu_3Ge, the interface planes are (0 0 1) and (0 1 0) planes respectively, and the viewing direction is [1 1 0] zone for both phases. **Figure 6(b)** shows the schematic illustration of the matching scenario at the interface. The atoms of sapphire within each lattice on (0 0 1) plane are located at the four corners of a rectangle (width = 4.759 Å, length = 8.243 Å), and the lattice of (0 1 0) plane Cu_3Ge

is also in rectangular shape (width = 4.54 Å, length = 4.22 Å). Therefore, two lattices of Cu_3Ge (0 1 0) plane match with one lattice of the c-sapphire (0 0 1) plane, as illustrated in **Figure 6(b)**. The lattice misfits of the width and length between two systems are ~4.60% and ~-2.33%, respectively. The interface region close to that of **Figure 6(a)** is enlarged for observation using HRTEM and shown in **Figure 6(c)**, to study the atomic structure in detail. The crystal planes of the film and the substrate connect with each other, but slightly bend around the misfit dislocations. Domain matching epitaxy (DME) [28–32] can be used to explain the matching of two phases, since no pseudomorphic Cu_3Ge has grown across the interface and the misfit strain is accommodated within several atomic layers at the interface. 9/8 and 8/7 domains alternate with a relative frequency of 0.5 to accommodate the misfit strain perpendicular to the interface, as shown in **Figure 6(c)**.

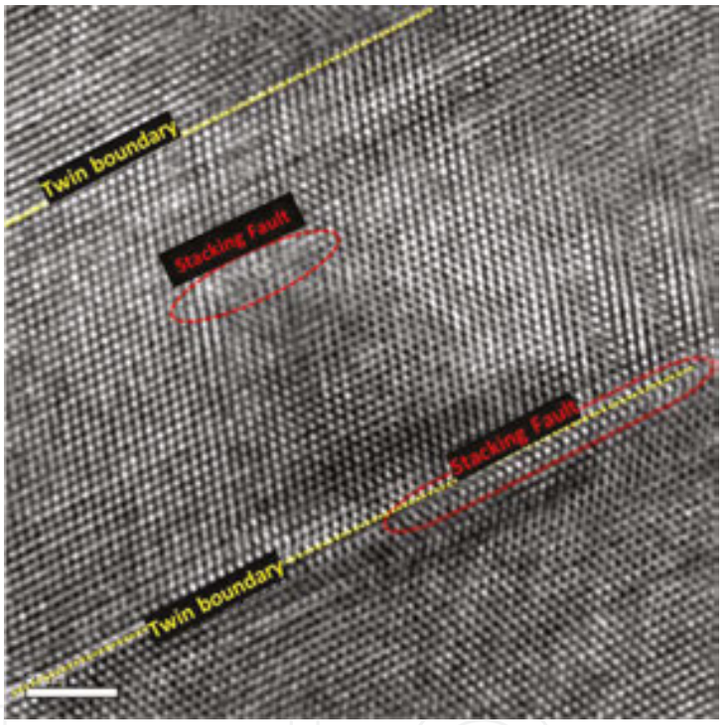

Figure 7 A typical HRTEM image showing the planar defects in Cu_3Ge thin film, in which twins and stacking faults coexist [42].

Planar defects, including twins and stacking faults (SF), are observed to exist in the as-grown epitaxial Cu_3Ge film and shown by HRTEM image (**Figure 7**). Extrinsic stacking fault is observed to exist close to the lower twin boundary (TB). Individual SF is observed within one grain. The densities of twins and SFs in the as-deposited Cu_3Ge film are close to that of pure Cu thin films with internal strain [33]. Previously in PLD-deposited films, deformation twins have been shown to be dominant [34]. Therefore, the concept of "generalized planar fault energies (GPFEs)" can explain the formation mechanism of the twins and SFs in the as-deposited Cu_3Ge film. In this concept, multiple intrinsic material properties, including stacking fault energy (SFE), unstable stacking fault energy (USFE), and unstable twin fault energy (UTE), play together to affect the twinning possibility [35]. Alloying elements have been

reported to lower the SFE of metals [36], and Cu alloy has been chosen to study twin interaction phenomena in previous studies [33] for the same reason. Thus, a leading partial Cu_3Ge is more likely to nucleate and slip due to a small energy barrier. Further, the combined effect of SFE, USFE, UTE, as well as the magnitude and orientation of the local shear stress determines whether the SF is annihilated, maintained, or transformed into a twin. If the nucleation and gliding barrier for the trailing partial is low, it will be easy to annihilate an SF. Due to the existence of SF in our films, the difference between USFE and SFE should be high for Cu_3Ge since it determines the energy barrier for the trailing partial to move. Therefore, stacking faults are generated by the movement of leading partials without trailing partials. Twins are then easily generated once a leading partial is emitted and an SF is formed, since the UTE is not quite higher than the USFE.

Grain size is another parameter to affect deformation twinning in nanocrystalline metals and alloys, in addition to GPFE curves. Deformation twinning is easiest at an optimum grain size [37]. Twins in metallic thin films have been reported to lead to excellent properties, including high electromigration resistance [35], high strength and ductility, good mechanical stability, and low electrical resistivity. They can also accommodate residual strains [38]. Furthermore, Cu_3Ge with twins will be a better metallization material as the twin boundaries will deter the diffusion.

The local work function of epitaxial Cu_3Ge thin film ϕ_{Cu3Ge} was measured by KPFM, showing the fundamental electronic property which affects both electron emission through the surface and electronic trajectories near the surface [39]. KPFM measures the work function of solid surfaces at atomic or molecular scales, demonstrating information about composition and electronic state of the local structures on the surface. When the conducting tip and the sample are brought in contact, a net electric current would flow between them until the Fermi levels are aligned. During measurement, a voltage is applied between tip and sample, consisting of a DC-bias and an AC-voltage:

$$V = \left(V_{DC} - V_{CPD}\right) + V_{AC}\, sin\left(\omega t\right) \tag{1}$$

where V_{CPD} is the contact potential difference between a conductive tip and a sample, $V_{AC}sin(\omega t)$ and V_{DC} are the applied AC voltages of frequency ω and DC voltage on the tip. The electrostatic force in a capacitor can be written as:

$$F = \frac{1}{2}\frac{dC}{dz}V^2 \tag{2}$$

where C is the tip-sample capacitance, z is the tip-sample distance, and V is the tip-sample voltage. Combining the above two equations, the electrostatic force can be split up into three contributions:

$$F = F_{DC} + F_{\omega} + F_{2\omega} \tag{3}$$

The DC component (F_{DC}) contributes to the topographical signal, the term F_{ω} measures the contact potential, and the contribution $F_{2\omega}$ can be used for capacitance microscopy. They can be expressed as following:

$$F_{dc} = \frac{dC}{dz}\left[\frac{1}{2}\left(V_{DC} - V_{CPD}\right)^2 + \frac{1}{4}V_{AC}^2\right] \tag{4}$$

$$F_{\omega} = \frac{-dC}{dz}\left(V_{DC} - V_{CPD}\right)V_{AC}\,sin\left(\omega t\right) \tag{5}$$

$$F_{2\omega} = \frac{-1}{4}\frac{dC}{dz}V_{AC}^2\,cos\left(2\omega t\right) \tag{6}$$

When $V_{DC} = V_{CPD}$, the electrostatic force component measured at frequency ω and the oscillating amplitude would be zero. Consequently, V_{DC} can track V_{CPD} at each point of the scan area using a feedback circuit. Once V_{CPD} is obtained, the local work function of Cu_3Ge thin film ϕ_{Cu3Ge} can be calculated as:

$$eV_{CPD} = \varphi_{tip} - \varphi_{Cu_3Ge} \tag{7}$$

where ϕ_{tip} is the work function of the conductive tip (~4.90 + 0.02 eV) [40], calibrated with a freshly cleaved highly oriented pyrolytic graphite (HOPG, Grade 1 SPI, 4.65 eV) [40] before the experiment. **Figure 8(a)** and **(b)** shows the topographical image and the corresponding surface potential image obtained for epitaxial Cu_3Ge thin film. Small grains of tens of nanometers can be seen clearly from the topographical image, while an almost uniform distribution of V_{CPD} within each grain was observed from the contact potential image. The "band profiles" derived from the middle regions (between two white dashed lines) of **Figure 8(a)** and **(b)** are shown in **Figure 8(c)** and **(d)**, demonstrating the height and V_{CPD} variation. The average V_{CPD} for epitaxial Cu_3Ge thin film was measured to be ~0.43 V. Therefore, the work function of Cu_3Ge thin film is:

$$\varphi_{Cu_3Ge} = \varphi_{tip} - eV_{CPD} = \left(4.9 \pm 0.02\right) - 0.43 = \left(4.47 \pm 0.02\right)eV \tag{8}$$

which is between the work functions of n^+ and p^+-polysilicon [41]. This value is desirable for epitaxial Cu_3Ge thin film to be used as a mid-gap gate metal even at very low temperatures for applications in CMOS devices, because it would require minimal and symmetric channel implants even at linewidths below 0.5 μm [41].

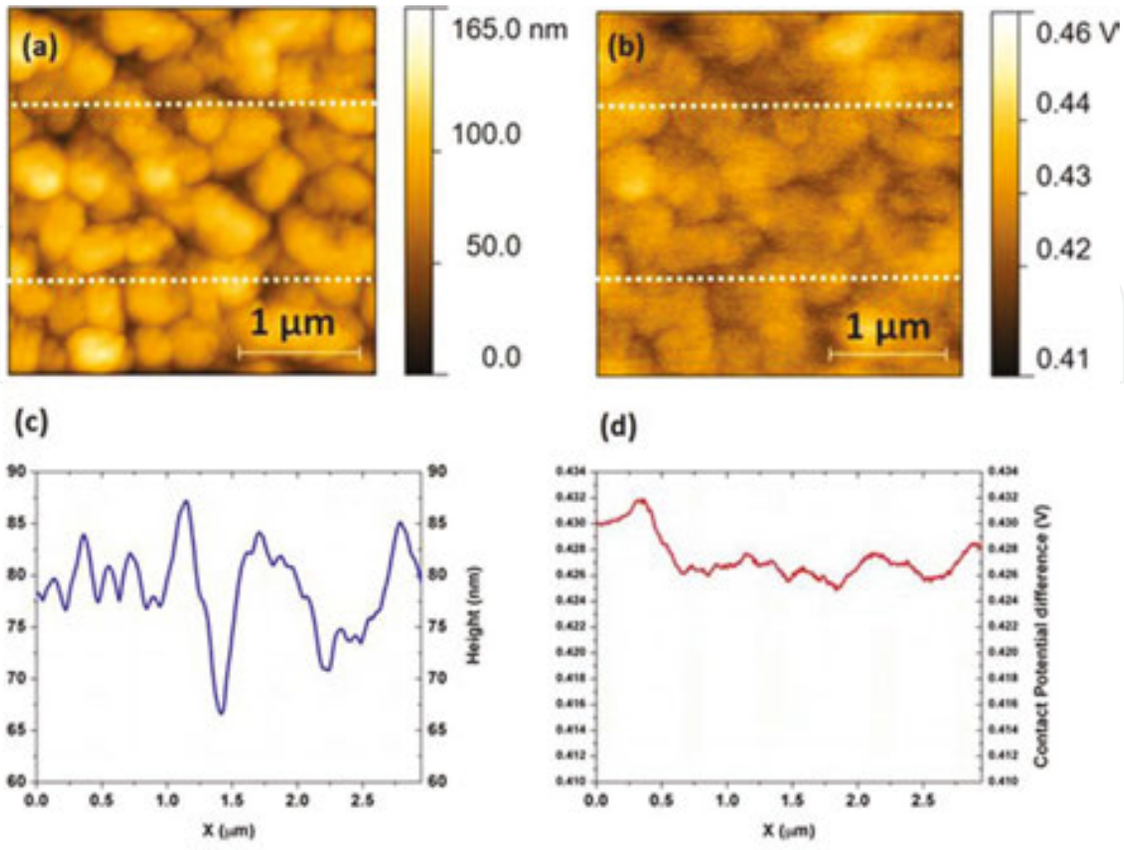

Figure 8. KPFM characterization of epitaxial Cu_3Ge thin film. (a) The topographical image, (b) the corresponding surface potential image, (c) the band profile derived from the middle region (between two white dashed lines) of (a) and (d) the band profile derived from the middle region (between two white dashed lines) of (b).

4. Conclusions

Epitaxial e_1-Cu_3Ge thin films are fabricated on *c*-plane sapphire substrate. The crystallinity of the as-grown e_1-Cu_3Ge thin film is improved, due to the modified deposition route. The e_1-Cu_3Ge phase (orthorhombic) is grown by the paradigm of domain matching epitaxy on *c*-plane sapphire, where two structures and their symmetries are completely different. In addition, twins are observed and studied in Cu_3Ge thin films, and their formation mechanism is explained by the concept of generalized planar fault energies (GPFEs). Twinning will reduce the diffusion of Cu and Ge atoms into the substrate or adjacent layers, and enhance the mechanical stability of Cu_3Ge thin films due to the improved strength and ductility and higher electromigration resistance. The average work function of epitaxial Cu_3Ge thin film is measured to be ~4.47 + 0.02 eV, rendering it a desirable mid-gap gate metal to be used for applications in CMOS devices. Therefore, the present epitaxial Cu_3Ge thin film with controlled crystallinity and defect structure is a promising candidate for the next-generation metallization material in the semiconductor industry.

Acknowledgements

FW and NY acknowledge the partial support by the National Science Foundation-MRSEC program through the Princeton Center for Complex Materials (DMR-0819860).

Author details

Fan Wu* and Nan Yao*

*Address all correspondence to: fanwu@princeton.edu and nyao@princeton.edu

Princeton Institute for the Science and Technology of Materials (PRISM), Princeton University, Princeton, New Jersey, USA

References

[1] Krusin-Elbaum L, Aboelfotoh MO. Unusually low resistivity of copper germanide thin films formed at low temperatures. Applied Physics Letters. 1991;58:1341–3.

[2] Doyle JP, Svensson BG, Aboelfotoh MO. Copper germanide Schottky barrier contacts to silicon. Journal of Applied Physics. 1996;80:2530–2.

[3] Huang JS, Huang SS, Tu KN, Deng F, Lau SS, Cheng SL, et al. Kinetics of Cu_3Ge formation and reaction with Al. Journal of Applied Physics. 1997;82:644–9.

[4] Borek MA, Oktyabrsky S, Aboelfotoh MO, Narayan J. Low resistivity copper germanide on (1 0 0) Si for contacts and interconnections. Applied Physics Letters. MRS Proceedings, Volume 514, 1996;69:3560–2.

[5] Aboelfotoh MO, Borek MA, Narayan J. Ohmic contact to p-type GaAs using Cu_3Ge. Applied Physics Letters. 1999;75:3953–5.

[6] Aboelfotoh MO, Oktyabrsky S, Narayan J, Woodall JM. Microstructure characterization of Cu_3Ge/n-type GaAs ohmic contacts. Journal of Applied Physics. 1994;76:5760–3.

[7] Aboelfotoh MO, Lin CL, Woodall JM. Novel low-resistance ohmic contact to n-type GaAs using Cu_3Ge. Applied Physics Letters. 1994;65:3245–7.

[8] Borek MA, Oktyabrsky S, Aboelfotoh MO, Narayan J. Properties of Cu_3Ge films for contacts to Si and SiGe and Cu metallization. In: Murarka SP, Eizenberg M, Fraser DB, Madar R, Tung R, editors. Advanced Interconnects and Contact Materials and Processes for Future Integrated Circuits; 1998. pp. 269–74.

[9] Aboelfotoh MO, Borek MA, Narayan J. Interaction of Cu and Cu_3Ge thin films with $Si_{1-x}Ge_x$ alloys. Applied Physics Letters. 1999;75:1739–41.

[10] Aboelfotoh MO, Tu KN, Nava F, Michelini M. Electrical transport properties of Cu_3Ge thin films. Journal of Applied Physics. 1994;75:1616–9.

[11] Guizzetti G, Marabelli F, Pellegrino P, Sassella A, Aboelfotoh MO. Optical response of Cu_3Ge thin films. Journal of Applied Physics. 1996;79:8115–7.

[12] Kumar D, Vispute RD, Aboelfotoh O, Oktyabrsky S, Jagannadham K, Narayan J, et al. $LaNiO_3$ and Cu_3Ge contacts to $YBa_2Cu_3O_{7-x}$ films. Journal of Electronic Materials. 1996;25:1760–6.

[13] Aboelfotoh MO, Borek MA, Narayan J. Microstructure and electrical resistivity of Cu and Cu_3Ge thin films on $Si_{1-x}Ge_x$ alloy layers. Journal of Applied Physics. 2000;87:365–8.

[14] Peter AP, Carbonell L, Schaekers M, Adelmann C, Meersschaut J, Franquet A, et al. Selective chemical vapor synthesis of Cu_3Ge: process optimization and film properties. Intermetallics. 2013;34:35–42.

[15] Hsin H-C, Lin W-T, Gong JR, Fang YK. Cu_3Ge Schottky contacts on n-GaN. Journal of Materials Science: Materials in Electronics. 2002;13:203–6.

[16] Liang HH, Luo JS, Lin WT. Room temperature oxidation of Cu_3Ge and $Cu^{-3}(Si_{1-x}Ge_x)$ on $Si_{1-x}Ge_x$. Materials Science in Semiconductor Processing. 2001;4:233–5.

[17] Nath P, Chopra KL. Electrical resistivity and thermoelectric power of copper germanium films. Thin Solid Films. 1979;58:339–43.

[18] Rao SS, Prater JT, Wu F, Nori S, Kumar D, Yue L, et al. Positive exchange bias in epitaxial permalloy/MgO integrated with Si (1 0 0). Current Opinion in Solid State and Materials Science. 2014;18:140–6.

[19] Rao SS, Prater J, Wu F, Shelton C, Maria J-P, Narayan J. Interface magnetism in epitaxial $BiFeO_3$-$La_{0.7}Sr_{0.3}MnO_3$ heterostructures integrated on Si (1 0 0). Nano Letters. 2013;13:5814–21.

[20] Lee Y, Wu F, Kumar R, Hunte F, Schwartz J, Narayan J. Epitaxial integration of dilute magnetic semiconductor Sr3SnO with Si (0 0 1). Applied Physics Letters. 2013;103:112101.

[21] Bayati M, Molaei R, Wu F, Budai J, Liu Y, Narayan R, et al. Correlation between structure and semiconductor-to-metal transition characteristics of VO_2TiO_2/sapphire thin film heterostructures. Acta Materialia. 2013;61:7805–15.

[22] Molaei R, Bayati R, Wu F, Narayan J. A microstructural approach toward the effect of thickness on semiconductor-to-metal transition characteristics of VO_2 epilayers. Journal of Applied Physics. 2014;115:164311.

[23] Lee Y, Wu F, Narayan J, Schwartz J. Oxygen vacancy enhanced room-temperature ferromagnetism in Sr3SnO/c-YSZ/Si (0 0 1) heterostructures. MRS Communications. 2014;4:7–13.

[24] Rao S, Prater J, Wu F, Nori S, Kumar D, Narayan J. Integration of epitaxial permalloy on Si (1 0 0) through domain matching epitaxy paradigm. Current Opinion in Solid State and Materials Science. 2013;18:1–5.

[25] Singamaneni SR, Prater J, Wu F, Narayan J. Interface magnetism of two functional epitaxial ferromagnetic oxides integrated with Si (1 0 0). Bulletin of the American Physical Society. APS March Meeting Abstracts, volume 1, page 1249, 2014.

[26] Singamaneni SR, Prater J, Wu F, Nori S, Kumar D, Yue L, et al. Positive exchange bias in epitaxial permalloy/MgO integrated with Si (1 0 0). Bulletin of the American Physical Society. APS March Meeting Abstracts, volume 1, page 1254, 2014.

[27] Wu F, Narayan J. Controlled epitaxial growth of body-centered cubic and face-centered cubic Cu on MgO for integration on Si. Crystal Growth & Design. 2013;13:5018–24.

[28] Narayan J, Larson BC. Domain epitaxy: a unified paradigm for thin film growth. Journal of Applied Physics. 2003;93:278–85.

[29] Wu F, Rao SS, Prater JT, Zhu YT, Narayan J. Tuning exchange bias in epitaxial Ni/MgO/TiN heterostructures integrated on Si(1 0 0). Current Opinion in Solid State and Materials Science. 2014;18:263–8.

[30] Singamaneni SR, Fan W, Prater JT, Narayan J. Magnetic properties of $BaTiO_3$/$La_{0.7}Sr_{0.3}MnO_3$ thin films integrated on Si(1 0 0). Journal of Applied Physics. Issue 22, pages 224–104, 2014;116.

[31] Bayati R, Molaei R, Richmond A, Nori S, Wu F, Kumar D, et al. Modification of properties of Yttria stabilized Zirconia epitaxial thin films by Excimer laser annealing. ACS Applied Materials & Interfaces. 2014;6:22316–25.

[32] Gbordzoe S, Kotoka R, Craven E, Kumar D, Wu F, Narayan J. Effect of substrate temperature on the microstructural properties of titanium nitride nanowires grown by pulsed laser deposition. Journal of Applied Physics. 2014;116:4310.

[33] Wu F, Wen HM, Lavernia EJ, Narayan J, Zhu YT. Twin intersection mechanisms in nanocrystalline fcc metals. Materials Science and Engineering: A. 2013;585:292–6.

[34] Wu F, Zhu YT, Narayan J. Grain size effect on twin density in as-deposited nanocrystalline Cu film. Philosophical Magazine. 2013;93:4355–63.

[35] Zhu YT, Liao XZ, Wu XL. Deformation twinning in nanocrystalline materials. Progress in Materials Science. 2012;57:1–62.

[36] Venables JA. The electron microscopy of deformation twinning. Journal of Physics and Chemistry of Solids. 1964;25:685–92.

[37] Wu XL, Zhu YT. Inverse grain-size effect on twinning in nanocrystalline Ni. Physical Review Letters. 2008;101:025503.

[38] Wu F, Zhu YT, Narayan J. Macroscopic twinning strain in nanocrystalline Cu. Materials Research Letters. 2014;2:63–9.

[39] Fain SC, McDavid JM. Work-function variation with alloy composition: Ag–Au. Physical Review B. 1974;9:5099–107.

[40] Yan F, Schoofs F, Shi J, Ha SD, Jaramillo R, Ramanathan S. Local charge writing in epitaxial $SmNiO_3$ thin films. Journal of Materials Chemistry C. 2014;2:3805–11.

[41] Aboelfotoh MO, Krusin-Elbaum L, Sun YC. Wet etching process with high selectivity between Cu and Cu_3Ge. Google Patents Publication number EP0769808 A3. 1997.

[42] Wu F, Zheng JK, Cai W, Yao N, Zhu YT, Narayan J. Fabrication of epitaxial Cu_3Ge on sapphire with controlled crystallinity and planar defects. Journal of Alloys and Compounds. 2015;641:238–43.